

Enhanced E \rightarrow Z Photoisomerisation in 2-Aminoazobenzene

José A. Gámez, Axel Koslowski and Walter Thiel

Theoretical non-adiabatic dynamics simulations at the semiempirical OM2/MRCI level reveal an enhanced E \rightarrow Z photoisomerisation for 2-aminoazobenzene. The E isomer contains an intramolecular hydrogen bond which weakens the azo N-N bond and thus facilitates isomerisation.

Azobenzene (AB) and its derivatives undergo ultrafast and reversible Z-E isomerisation upon light irradiation. Azobenzene has thus been utilised as a light-activated switch in a variety of polymers¹ and molecular machines² and for the design of polymers with light-controlled viscosity.³⁻⁵ Besides, the molecular motion associated to isomerisation has been exploited in AB-based synthetic materials that can undergo photocontraction⁶ and so produce mechanical work.^{7, 8}

It is well established that this reaction involves two low-lying singlet excited states, namely S_1 and S_2 . These states show different quantum yields,⁹ violating Kasha's rule. Steady-state measurements of the E \rightarrow Z isomerisation in hexane reported yields of 0.20-0.27 for S_1 excitation, but only of 0.09-0.12 for S_2 excitation.¹⁰⁻¹² The reverse Z \rightarrow E process also has a higher quantum yield for S_1 (0.55-0.68) than for S_2 (0.40-0.44).¹³⁻¹⁵ In the present work we will focus, consequently, on the photoisomerisation of the S_1 state, with the most efficient Z-E interconversion. The S_1 state is also relevant because selective excitation to either S_1 or S_2 can be utilized to control the major isomer in the photostationary state.^{10, 16} Moreover, its study may help rationalize the differences in the observed quantum yields for photoisomerisations starting in the S_1 and S_2 states.

The S_1 state is associated with a symmetry-forbidden $n-\pi^*$ transition in the visible region.¹⁷⁻¹⁹ Initially it was assumed to undergo inversion by a change in the CNN angle at a fixed CCNN dihedral.^{11, 16, 20-22} It was later suggested that the photoisomerisation should proceed mainly by rotation of the phenyl rings around the N-N bond.²³⁻²⁷ More recently, a new mechanism has been proposed where the driving force of the reaction is actually the rotation of the N_2 motif rather than the movement of the rings.²⁸⁻³² This latter mechanism is also supported by our recent work on the photoisomerization of AB and 4-aminoazobenzene (4-aAB).³²⁻³⁴ By analyzing periodic features in the excited-state population decay, we identified the N_2 rotation as the coordinate driving the reaction.

Attempts to modify the outcome of the photoisomerisation of AB have been made by means of substitution. Sub-picosecond time-resolved absorption spectra on push-pull p,p'-substituted AB shows that S_2 isomerisation in these compounds is different

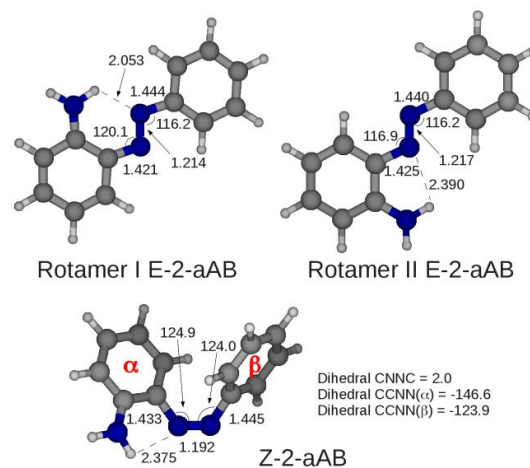


Fig. 1 Optimized geometries for the rotamers of E-2-aAB (top) and Z-2-aAB (bottom) at the OM2/MRCI(12,11) level of theory. Bond lengths are given in Å and angles in degree.

from that in the parent AB.³³ A 2-hydroxyAB (2-hAB) derivative (Orange II) with an intramolecular hydrogen bond (IHB) between the $-OH$ group and the azo-nitrogen atom tautomerises upon irradiation by an ultrafast proton transfer to the corresponding phenyl-hydrazone, which has a weak N-N bond and thus exhibits a very fast isomerisation but also a complex decay profile.³⁴ 2,2'-diaminoazobenzene derivatives have been also reported.³⁵ Such molecules, with several IHBs, show fluorescence and no light-induced isomerisation. Photoisomerisation is found again after alkylation of the $-NH_2$ groups, which prevents formation of IHBs.

In the present communication, we investigate the mechanism of the photoisomerisation of 2-aminoazobenzene (2-aAB) by means of semiempirical (OM2/MRCI) non-adiabatic dynamical simulations. We expect that with only one IHB the isomerisation process will not be hindered. 2-aAB and 2-hAB should behave differently as the former is not as prone to tautomerisation.

There are two rotamers for the E isomer of 2-aAB (Fig. 1). They are nearly degenerate, with a rotation barrier of 5 kcal mol⁻¹ that prevents spontaneous interconversion (see Supporting Information). The smallest distance between an $-NH_2$ hydrogen and an azo nitrogen atom is much smaller for rotamer I (2.053 Å) than for rotamer II (2.390 Å), suggesting a much weaker IHB in the latter. Several bonding analysis techniques (NCI plots, QTAIM and NBO, see Supporting Information) confirm this assessment. The Z isomer presents a unique rotamer (Fig. 1) with

a CNNC dihedral near 0° . The resulting steric strain is alleviated by rotating the phenyl rings by ca. 20° around the C-N bonds. The distances between the amino hydrogen and azo nitrogen atoms are again quite long (at least 2.375 \AA), indicating a weak, if any, IHB. The twist of the phenyl rings in the Z isomer is the source of helical chirality, leading to *M*- or *P*-helicity (see Supporting Information for definitions). Likewise, after photoexcitation, *M*- or *P*-helical minimum-energy conical intersections (MECIs) can be reached. Consequently, the helical chirality will tend to be conserved for the $Z \rightarrow E$ isomerisation. The same was found for AB and 4-aAB.³⁶⁻³⁸ Eight MECIs were located for 2-aAB, four for each rotamer. They all lie within an energy window of 2 kcal mol^{-1} and have similar geometries, characterised mainly by a CNNC dihedral close to 100° and CCNN dihedrals close to 0° (see Supporting Information for more details).

All our trajectories were started from the *M*-helical structure. As anticipated, there is a tendency to preserve the helical chirality in the $Z \rightarrow E$ reaction (Fig. 2). This is so because this pathway is lower in energy than the alternative one that does not preserve chirality (see Supporting Information). By contrast, in the inverse $E \rightarrow Z$ process the trajectories reach the *M*- and *P*-helical MECIs almost equally well (see Supporting Information), as anticipated because of the near planarity of both rotamers of E-2-aAB.

Table 1 summarises the quantum yields and the S_1 mean life times computed for the photoisomerisation of 2-aAB. The yields are 57 % for the $Z \rightarrow E$ process, and 19% (17 %) for the $E \rightarrow Z$ isomerisation starting from rotamer I (II). They are not higher than those computed for 4-aAB or AB (see Table 1). The average $Z \rightarrow E$ hopping times are the same for 2-aAB and 4-aAB (63 fs), 14 % smaller than for the parent azobenzene (72 fs). The speed-up for 4-aAB has previously been attributed to the increased energy gap between the Franck-Condon (FC) region and the MECI.³⁸ This explanation also holds in the present case: the FC-MECI gaps of 2- and 4-aAB are similar (31 and 30 kcal mol^{-1} , respectively) and larger than that of AB (27 kcal mol^{-1}). An even larger speed-up is observed in the $E \rightarrow Z$ reaction of 2-aAB. The mean decay times for rotamers I and II (156 and 196 fs, respectively) are significantly shorter than those for 4-aAB (223 fs) and the parent AB molecule (258 fs), with a maximum speed-up of 40%. The shorter decay times of 2-aAB relative to 4-aAB cannot be explained by means of the FC-MECI gap, which is similar in both systems (25 and 23 kcal mol^{-1} for rotamers I and II of 2-aAB versus 25 kcal mol^{-1} for 4-aAB). We note, however, that rotamer I of E-2-aAB has a strong N-H...N interaction that is much weaker in rotamer II and absent in the *para* derivative. This strong IHB will polarise the lone-pair of the involved azo nitrogen atom and weaken the N-N bond. This notion is confirmed by the analysis of the Electron Localisation Function (ELF), which indicates the most likely location of electron pairs in a molecule,^{39, 40} e.g. in terms of core, bonding or non-bonding (lone) pairs.

Table 2 shows the population of some relevant valence electron pairs (i.e., basins in ELF terminology) for the E-form of AB, rotamer I of 2-aAB, and 4-aAB. Data are given for the S_0 state at its optimized geometry and for the S_1 state at the FC geometry ($S_{1\text{vert}}$). The disynaptic $V(N-N')$ basin represents the bonding pairs responsible for the azo N-N bond. The smallest population of this basin is found for I-2-aAB, which is thus

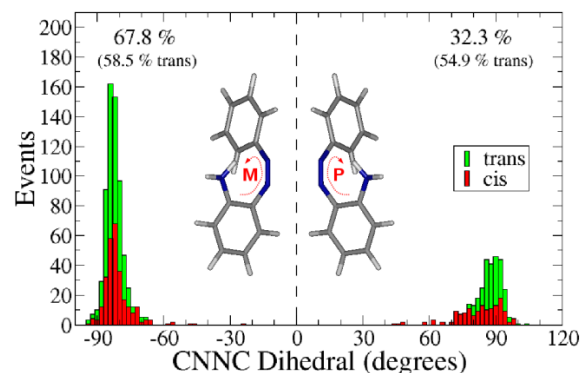


Fig. 2 Distribution of CNNC dihedral angles at the hopping point to the ground state for the $Z \rightarrow E$ photoisomerization of 2-aAB.

Table 1 Quantum yield (%) and S_1 mean life time (fs) for the $Z \rightarrow E$ and $E \rightarrow Z$ photoisomerisations of AB, 4-aAB, and 2-aAB; in the $E \rightarrow Z$ case, results are given for both E rotamers (I-2-aAB and II-2-aAB).

	$Z \rightarrow E$			$E \rightarrow Z$			
	AB	4-aAB	2-aAB	AB	4-aAB	I-2-aAB	II-2-aAB
quantum yield	58	60	57	17	15	19	17
S_1 mean life	72	63	63	258	223	156	196

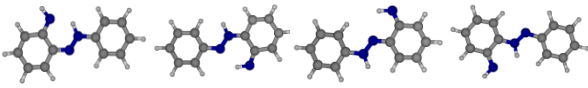
associated with the weakest N-N bond. This weakening is caused by the polarisation of the lone-pair of the azo nitrogen atom upon IHB formation. The monosynaptic $V(N')$ basin corresponding to this lone-pair has indeed the largest population in I-2-aAB. This trend is kept upon excitation to S_1 , where I-2-aAB again shows the least populated $V(N-N')$ and largest populated $V(N')$ basins and, hence, the weakest N-N bond. In rotamer II, the speed-up is smaller (see Table 1) and cannot be rationalized by an analogous ELF analysis. In any event, when targeting 2-aAB-based compounds with the fastest $E \rightarrow Z$ photoisomerisation, one should design molecules where rotamer II is strongly destabilised with respect to rotamer I, which should be possible through proper further substitution of the phenyl ring (e.g., in 6-position). We also note that the activation of the N-N azo bond in 2-aAB is reminiscent of the situation in 2-hAB, where an excited-state intramolecular proton transfer (ESIPT) leads to the formation of a covalent N-H bond (instead of just a hydrogen bond) and the conversion of the azo double bond to a formal single bond.

As found for AB and 4-aAB, 2-aAB features an oscillatory

Table 2 ELF basin populations (in e) calculated with the B3LYP/6-311++G(3df,2p) density for E-AB, rotamer I of E-2-aAB, and E-4-aAB. N denotes the nitrogen atom directly linked to the phenyl ring bearing the $-\text{NH}_2$ group, while N' is the other nitrogen atom of the N-N bond. S_0 refers to the ground-state density calculated at the ground-state geometry, and $S_{1\text{vert}}$ is the S_1 density calculated at the geometry of the ground-state minimum.

	AB		I-2-aAB		4-aAB	
	S_0	$S_{1\text{vert}}$	S_0	$S_{1\text{vert}}$	S_0	$S_{1\text{vert}}$
$V(N-N')$	2.3059	1.7656	2.2309	1.6877	2.2735	1.7240
$V(N-C)$	2.0818	1.9470	2.0769	1.8862	2.0856	1.9146
$V(N'-C')$	2.0818	1.9470	2.1544	1.9784	2.1088	1.9687
$V(N)$	2.7223	2.9893	2.7095	3.0192	2.7745	3.0667
$V(N')$	2.7223	2.9893	2.8442	3.1801	2.7282	3.0027

Table 3 Energy difference (in kcal mol⁻¹) between all possible hydrazone tautomers of E-2-aAB and rotamer I of E-2-aAB in the S₀ and S₁ states.



	I-HYZ-I	I-HYZ-II	II-HYZ-I	II-HYZ-II
S ₀	14	38	26	32
S ₁	Deprotonation ^a	33	25	26

^a The S₁ I-HYZ-I state undergoes an ESIPT that leads back to the azo tautomer.

decay to the ground state, both in the Z → E and the E → Z channels. Periods of frequent hops to the ground state alternate with periods of few or no hops. As already discussed for AB and 4-aAB,³⁶⁻³⁸ the Fourier transform of the function describing this periodic decay reveals that this oscillatory approach is caused by the rotation of the N₂ motif (see Supporting Information for further details). The photoisomerisation of 2-aAB thus follows the same basic mechanism as 4-aAB and AB: it is the rotation of the N-N bond which induces the movement of the phenyl rings and eventually triggers the isomerisation of the molecule, rather than an actual rotation of the phenyl rings. This common pathway for AB, 4-aAB, and 2-aAB could explain the invariance of the quantum yield upon substitution.

This mechanism is completely different from the one observed in 2-hAB derivatives,³⁴ where photoexcitation causes an ESIPT that yields the corresponding phenyl-hydrazone. This tautomer isomerises fast and forms a photoproduct in the excited state, which then decays to the S₀ state by fluorescence emission, without recovering the azo tautomer of 2-hAB. The situation is different in 2-aAB: here, the hydrazones are less stable than the azo tautomers both in the S₀ and S₁ state (Table 3), and they are not observed during our dynamical simulations, which yield the Z isomer of 2-aAB through an ultrafast radiationless process. Hence, 2-aAB derivatives may act as efficient photoswitches, contrary to seemingly analogous 2-hAB compounds.

In conclusion, we report simulations of 2-aAB, which show faster photoisomerisation than the parent AB compound, specifically for E → Z conversion. This enhancement can be attributed to the IHB in the rotamer I of E-2-aAB, which polarises the lone-pair of the azo nitrogen atom and thus weakens the N-N bond. 2-aAB derivatives may thus serve as fast photoswitches, unlike 2-hAB compounds. It seems possible that the speed of their photoisomerisation can be further enhanced by substituent design.

JAG acknowledges the Alexander von Humboldt Stiftung for a postdoctoral fellowship.

Notes and references

^a Max-Planck-Institut für Kohlenforschung, Kaiser-Wilhelm-Platz, 1. 45470 Mülheim an der Ruhr, Germany. Fax: +49 208 306 2996; Tel: +49 208 306 2150; E-mail: thiel@kofo.mpg.de

† Electronic Supplementary Information (ESI) available. Computational methods. Energy profile along the CCNN dihedral angle for E-2-aAB. Bonding analysis for 2-aAB. Geometries of the MECIs of 2-aAB. Definition of helical chirality in Z-2-aAB. LIIC between the FC and MECI for Z-2-aAB. Distribution of CNNC dihedral angles at hopping points for E → Z photoisomerization of 2-aAB. Distribution of hopping events with respect to the time for photoisomerisation of 2-aAB. See DOI: 10.1039/b000000x/

1. F. Puntoriero, P. Ceroni, V. Balzani, G. Bergamini and F. Vögtle, *J. Am. Chem. Soc.*, 2007, **129**, 10714-10719.
2. T. Muraoka, K. Kinbara and T. Aida, *Nature*, 2006, **440**, 512-515.
3. S. Tamesue, Y. Takashima, H. Yamaguchi, S. Shinkai and A. Harada, *Angew. Chem. Int. Ed.*, 2010, **49**, 7461-7464.
4. S. Yagai, T. Nakajima, K. Kishikawa, S. Kohmoto, T. Karatsu and A. Kitamura, *J. Am. Chem. Soc.*, 2005, **127**, 11134-11139.
5. H. Sakai, Y. Orihara, H. Kodashima, A. Matsumura, T. Ohkubo, K. Tsuchiya and M. Abe, *J. Am. Chem. Soc.*, 2005, **127**, 13454-13455.
6. Y. Yu, M. Nakano and T. Ikeda, *Nature*, 2003, **425**, 145-145.
7. N. B. Holland, T. Hugel, G. Neuert, A. Cattani-Scholz, C. Renner, D. Oesterhelt, L. Moroder, M. Seitz and H. E. Gaub, *Macromolecules*, 2003, **36**, 2015-2023.
8. T. Hugel, N. B. Holland, A. Cattani, L. Moroder, M. Seitz and H. E. Gaub, *Science*, 2002, **296**, 1103-1106.
9. M. Kasha, *Discuss. Faraday Soc.*, 1950, **9**, 14-19.
10. G. Zimmerman, L.-Y. Chow and U.-J. Paik, *J. Am. Chem. Soc.*, 1958, **80**, 3528-3531.
11. H. Rau, *J. Photochem.*, 1984, **26**, 221-225.
12. P. Bortolus and S. Monti, *J. Phys. Chem.*, 1979, **83**, 648-652.
13. N. Siampiringue, G. Guyot, S. Monti and P. Bortolus, *J. Photochem.*, 1987, **37**, 185-188.
14. J. Ronayette, R. Arnaud, P. Lebourgeois and J. Lemaire, *Can. J. Chem.*, 1974, **52**, 1848-1857.
15. H. Stegemeyer, *J. Phys. Chem.*, 1962, **66**, 2555-2560.
16. H. Rau and E. Lueddecke, *J. Am. Chem. Soc.*, 1982, **104**, 1616-1620.
17. H. H. Jaffe and M. Orchin, *Theory and Application of Ultraviolet Spectroscopy*, Wiley, New York, 1962.
18. H. Rau, *Angew. Chem. Int. Ed.*, 1973, **12**, 224-235.
19. H. Bisle, M. Römer and H. Rau, *Ber. Bunsenges. Physik. Chem.*, 1976, **80**, 301-305.
20. P. Cattaneo and M. Persico, *Phys. Chem. Chem. Phys.*, 1999, **1**, 4739-4743.
21. S. Monti, G. Orlandi and P. Palmieri, *Chem. Phys.*, 1982, **71**, 87-99.
22. N. Biswas and S. Umaphathy, *Chem. Phys. Lett.*, 1995, **236**, 24-29.
23. C. Ciminelli, G. Granucci and M. Persico, *Chem. – Eur. J.*, 2004, **10**, 2327-2341.
24. A. Cembran, F. Bernardi, M. Garavelli, L. Gagliardi and G. Orlandi, *J. Am. Chem. Soc.*, 2004, **126**, 3234-3243.
25. I. Conti, M. Garavelli and G. Orlandi, *J. Am. Chem. Soc.*, 2008, **130**, 5216-5230.
26. C. Ciminelli, G. Granucci and M. Persico, *J. Chem. Phys.*, 2005, **123**, 174317.
27. A. Toniolo, C. Ciminelli, M. Persico and T. J. Martínez, *J. Chem. Phys.*, 2005, **123**, 234308.
28. T. Pancur, F. Renth, F. Temps, B. Harbaum, A. Kruger, R. Herges and C. Nather, *Phys. Chem. Chem. Phys.*, 2005, **7**, 1985-1989.
29. M. Böckmann, N. L. Doltsinis and D. Marx, *Phys. Rev. E*, 2008, **78**, 036101.
30. M. Böckmann, N. L. Doltsinis and D. Marx, *J. Phys. Chem. A*, 2009, **114**, 745-754.
31. M. Böckmann, D. Marx, C. Peter, L. D. Site, K. Kremer and N. L. Doltsinis, *Phys. Chem. Chem. Phys.*, 2011, **13**, 7604-7621.
32. T. Cusati, G. Granucci and M. Persico, *J. Am. Chem. Soc.*, 2011, **133**, 5109-5123.
33. M. Hagiri, N. Ichinose, C. Zhao, H. Horiuchi, H. Hiratsuka and T. Nakayama, *Chem. Phys. Lett.*, 2004, **391**, 297-301.
34. A. Douhal, M. Sanz and L. Tormo, *Proc. Natl. Acad. Sci. U. S. A.*, 2005, **102**, 18807-18812.
35. H. M. D. Bandara, T. R. Friss, M. M. Enriquez, W. Isley, C. Incarvito, H. A. Frank, J. Gascon and S. C. Burdette, *J. Org. Chem.*, 2010, **75**, 4817-4827.
36. O. Weingart, Z. Lan, A. Koslowski and W. Thiel, *J. Phys. Chem. Lett.*, 2011, **2**, 1506-1509.
37. J. A. Gamez, O. Weingart, A. Koslowski and W. Thiel, *J. Chem. Theory Comput.*, 2012, **8**, 2352-2358.
38. J. A. Gamez, O. Weingart, A. Koslowski and W. Thiel, *Phys. Chem. Chem. Phys.*, 2013, **15**, 11814-11821.
39. A. D. Becke and K. E. Edgecombe, *J. Chem. Phys.*, 1990, **92**, 5397-5403.
40. B. Silvi and A. Savin, *Nature*, 1994, **371**, 683-686.